HHS Public Access

Author manuscript

NMR Biomed. Author manuscript; available in PMC 2020 June 01.

Published in final edited form as:

NMR Biomed. 2019 June ; 32(6): e4091. doi:10.1002/nbm.4091.

Metabolism of hyperpolarized ^{13}C-acetoacetate to β-hydroxybutyrate detects real-time mitochondrial redox state and dysfunction in heart tissue

Wei Chen[1,#], **Gaurav Sharma**[1,#], **Weina Jiang**[1], **Nesmine R. Maptue**[1], **Craig R. Malloy**[1,2,3,4], **A. Dean Sherry**[1,2,5], and **Chalermchai Khemtong**[1,2,*]

[1]Advanced Imaging Research Center, University of Texas Southwestern Medical Center, Dallas, TX, USA;

[2]Department of Radiology, University of Texas Southwestern Medical Center, Dallas, TX, USA;

[3]Department of Internal Medicine, University of Texas Southwestern Medical Center, Dallas, TX, USA;

[4]VA North Texas Health Care System, Dallas, TX, USA;

[5]Department of Chemistry, University of Texas at Dallas, Richardson, TX, USA

Abstract

Mitochondrial dysfunction is considered to be an important component of many metabolic diseases yet there is no reliable imaging biomarker for monitoring mitochondrial damage *in vivo*. A large prior literature on inter-conversion of β-hydroxybutyrate (β-HB) and acetoacetate (AcAc) indicates that the process is mitochondrial and the ratio reflects specifically mitochondrial redox state. Therefore the conversion of [1,3-^{13}C]AcAc to [1,3-^{13}C]β-HB is expected to be sensitive to the abnormal redox state present in dysfunctional mitochondria. In this study, we examined conversion of hyperpolarized (HP) ^{13}C-acetoacetate (AcAc) to ^{13}C-β-hydroxybutyrate (β-HB) as a potential imaging biomarker for mitochondrial redox and dysfunction in perfused rat hearts. Conversion of HP AcAc to β-HB was investigated using ^{13}C magnetic resonance spectroscopy (MRS) in Langendorff-perfused rat hearts in four groups: control, global ischemic reperfusion, low-flow ischemic, and rotenone (mitochondrial complex-I inhibitor) treated hearts. We observed that more β-HB was produced from AcAc in ischemic hearts and the hearts exposed to complex I inhibitor, rotenone, compared to controls consistent with accumulation of excess mitochondrial NADH. The increase in β-HB, as detected by ^{13}C MRS, was validated by a direct measure of tissue β-HB by ^{1}H nuclear magnetic resonance (NMR) in tissue extracts. The redox ratio, NAD^+/NADH, measured by enzyme assays of homogenized tissue, also paralleled production of β-HB from AcAc. Transmission electron microscopy of tissues provided direct evidence for abnormal mitochondrial structure in each ischemic tissue model. The results suggest that conversion of HP-

[*]**Correspondence:** Chalermchai Khemtong, University of Texas Southwestern Medical Center, 5323 Harry Hines Boulevard, Dallas, TX 75390-8568, USA. Phone: +1 (214) 645-2772; charlie.khemtong@utsouthwestern.edu.
[#]These authors contributed equally to this article.

Declarations of Interest
None

AcAc to HP-β-HB detected by ^{13}C-MRS may serve as a useful diagnostic marker of mitochondrial redox and dysfunction in heart tissue *in vivo*.

Graphical abstract

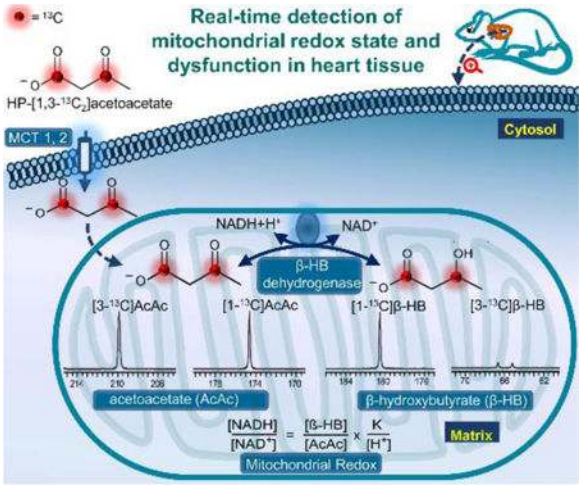

We explored the conversion of hyperpolarized [1,3-^{13}C]acetoacetate to to ^{13}C-β-hydroxybutyrate as a potential imaging biomarker for mitochondrial redox in perfused rat hearts. Our results show that the production of hyperpolarized β-hydroxybutyrate from hyperpolarized acetoacetate was much higher in ischemic and rotenone-treated hearts, reflecting the increased concentration of NADH under this reduced state. The redox-dependent conversion between this metabolic pair in mitochondria may lead to the development of an imaging tool for redox imaging of the heart by hyperpolarized ^{13}C MRI.

Keywords

mitochondrial redox; mitochondrial dysfunction; acetoacetate; β-hydroxybutyrate; hyperpolarized ^{13}C-MR

1. Introduction

Mitochondria are recognized as crucial targets and regulators of cardiac injury during ischemia and reperfusion[1]. The role of mitochondria is essential in metabolism and maintaining energy homeostasis as they synthesize the majority of ATP and biosynthetic intermediates needed for cell growth and function. Dysfunctional mitochondria and impaired energy homeostasis are intricately linked with heart failure and several other high impact diseases including type 2 diabetes, cancer, and neurodegenerative diseases [2–5]. One important biomarker of dysfunctional mitochondria is abnormal cell redox so this has become an attractive imaging target. The nicotinamide adenine dinucleotide redox pair, NAD^+ and NADH play key roles in regulating mitochondrial redox [6]. Disruption of the electron transport chain can result in accumulation of excess mitochondrial NADH so a measure of the mitochondrial NAD^+/NADH ratio is an important imaging target. Only a few imaging methods have been reported for assessment of mitochondrial redox *in vivo*. Most

mitochondrial NADH is tightly bound to protein [7] so the ratio of NAD^+ to NADH measured in tissue extracts does not necessarily reflect tissue redox.

To overcome this limitation, the reactions catalyzed by cytosolic lactate dehydrogenase (LDH) and mitochondrial β-hydroxybutyrate dehydrogenase (β-HBDH) have been widely used to estimate cytosolic and mitochondrial NAD^+/NADH ratios, respectively. These ratios are derived from enzyme-based analytical measures of pyruvate, lactate, acetoacetate, and β-hydroxybutyrate in tissue extracts and the known equilibrium constants for these reactions [8–11]. A variety of optical methods have also been used to measure NADH levels in tissues. Chance *et al.* pioneered fluorescence methods [12–14] while Asfour *et al.* used a high-speed CCD camera to measure fluorescence signal of NADH in isolated working rabbit hearts [15]. Raman spectroscopy has also been used to measure the redox state of cytochromes involved in the electron transport chain in isolated, perfused rat hearts [16]. Optical methods such as these are powerful but have been limited so far to cells, isolated organs, and small rodents where light penetration is not a limiting factor.

There has been growing interest in employing hyperpolarized (HP) ^{13}C magnetic resonance imaging to characterize cellular metabolism and detect metabolic abnormalities *in vivo* [17–19]. Using this technology, the ^{13}C NMR signal of any ^{13}C-enriched metabolic substrate can be increased by over 10,000-fold by prealtering the spin state of the molecule using dynamic nuclear polarization (DNP).[20] With such improved NMR sensitivity, the ^{13}C NMR signals of the substrate and subsequent metabolic products can be imaged at a temporal resolution of seconds. Recently, Christensen, *et al.* [21] reported a measure of cytosolic NAD^+/NADH based upon quantitative measures of the NMR signals of HP-pyruvate and HP-lactate generated from HP-glucose in human breast cancer and prostate cancer cells. Similarly, Spielman, *et al.* [22] demonstrated that more HP-lactate is produced from HP-pyruvate in livers of rats given a prior injection of ethanol and concluded that conversion of HP-pyruvate to HP-lactate may provide an indirect in vivo assay of cytosolic NADH levels. Park *et al.* confirmed the increased cytosolic NADH levels in ethanol-treated rat livers from the increased HP-lactate to HP-pyruvate ratio measured after injections of HP-alanine [23].

In this study, we explored the conversion of HP [1,3-^{13}C]acetoacetate (AcAc) to HP-[1,3-^{13}C]β-hydroxybutyrate (β-HB) as a possible biomarker of mitochondrial redox status in isolated perfused rat hearts. Conversion of acetoacetate to β-hydroxybutyrate is catalyzed by β-hydroxybutyrate dehydrogenase (β-HBDH), an enzyme present on the inner mitochondrial membrane (Fig. 1). Given that NADH is a required cofactor, we hypothesized that conversion of HP-AcAc to HP-β-HB should reflect mitochondrial NADH. To test this hypothesis, we measured the real-time conversion of HP-[1,3-^{13}C]AcAc to HP-[1,3-^{13}C]β-HB in isolated perfused rat hearts after experiencing a period of global ischemia reperfusion, low-flow ischemia, or treatment with the complex I inhibitor, rotenone. Greater production of HP-β-HB was observed by ^{13}C NMR in all ischemic and treated hearts compared to control hearts. The observed results were supported by independent measures of tissue β-HB by ^1H NMR, the tissue NAD^+/NADH ratio as measured enzymatically, and altered mitochondria structures as detected by transmission electron microscopy.

2. Methods

2.1 Preparation and hyperpolarization of [1,3-^{13}C]acetoacetate

[1,3-^{13}C]Acetoacetate was prepared by hydrolysis of ethyl [1,3-^{13}C]acetoacetate (Cambridge Isotope Laboratories, Tewksbury, MA) using 5 M NaOH warmed to 45 °C for 45 min (Fig. 2a). The resulting [1,3-^{13}C]sodium acetoacetate solution was first neutralized and then mixed with glycerol (1:1, v/v), OX063 trityl radical (GE Healthcare, 15 mM) and Gadoteridol ([Gd^{3+}] = 2 mM) and polarized at ~1.4 K in a HyperSense polarizer (Oxford Instruments) for 2 h. For T_1 analysis and ^{13}C signal enhancement measurement, the polarized sample was dissolved in superheated water (4 mL) and rapidly transferred into a 10 mm NMR tube placed in a 10-mm NMR probe tuned to ^{13}C (9.4 T, Agilent). A series of ^{13}C NMR spectra were acquired every 5 s with a 10-deg flip angle. T_1 relaxation rates and ^{13}C signal enhancements were measured using previously reported methods [25]. For perfused heart studies, [1,3-^{13}C]acetoacetate was prepared and polarized under the same conditions. Dissolution of the polarized sample was done using superheated PBS solution (pH = 7.4). Final pH of the resulting HP ^{13}C-AcAc solution was well within the physiological range (pH = 7.3 ± 0.2, n = 16 dissolutions).

2.2 Perfusion conditions, DNP, and ^{13}C MRS

Animal studies were approved by the Institutional Animal Care and Use Committee (IACUC) at UT Southwestern Medical Center. Hearts were obtained from healthy male Sprague-Dawley rats (~400 g). The isolated hearts were retrograde perfused as described previously [26]. Briefly, hearts were rapidly excised from the animals under general anesthesia (1.5% isoflurane) and arrested in ice-cold saline. The hearts were then perfused at a constant pressure (100 cm H_2O) with a modified phosphate-free Krebs Henseleit (P_i-free KH) buffer containing a physiological mixture of glucose (5.5 mM), lactate (1.2 mM), pyruvate (0.12 mM), and mixed long-chain free fatty acids (0.4 mM) with 0.75% bovine serum albumin. Specifically, free fatty acids were a mixture of palmitic acid (23.7 mole %), palmitoleic acid (5.6 mole %), stearic acid (2.6 mole %), oleic acid (26.3 mole %), linoleic acid (37.0 mole %), γ-linoleic acid (2.4 mole %), and docosahexaenoic acid (2.3 mole %). The perfusion buffer was oxygenated with a 95:5 mixture of O_2/CO_2. A balloon was inserted into the left ventricle for heart rate and developed pressure readouts. The perfused heart was placed into a 20-mm NMR tube and the perfusion apparatus was then placed into the bore of a 9.4 T spectrometer. Shimming was carried out on the ^{23}Na FID to a linewidth of ~18 Hz while the heart was surrounded by a sucrose flush (250 mM) to remove extracellular ^{23}Na. After ~20 min of perfusion, hearts were either made ischemic or treated with rotenone for 30 min prior to the HP experiment. In the global ischemia reperfusion hearts, the flow of perfusate was completely occluded while in the low-flow ischemia group, the perfusion pressured was lowered to 25 cm H_2O. In rotenone-treated hearts, rotenone was added to the perfusion media (20 μM). In all four groups, the heart rate (HR), coronary flow (CF), developed pressure, and oxygen partial pressure (pO_2) were measured at ~20 minutes as a baseline and again at ~45 min.

^{31}P NMR spectra of each heart were acquired using a 90-degree flip angle (number of transients = 64). The ^{31}P chemical shift scale was referenced to phosphocreatine (PCr) set to

0 ppm. Intracellular pH of the hearts was measured from the chemical shift of the inorganic phosphate (P_i) peak using a modified Henderson–Hasselbalch equation, pH = 6.72 + $log[(\delta P_i\text{-}3.17)/(5.72\text{-}\delta P_i)]$, as described previously[27]. After ~50 min of shimming and ^{31}P NMR measurements, polarized samples of [1,3-^{13}C]AcAc were rapidly dissolved in superheated PBS solution (pH = 7.4, 4 mL). A 3-mL aliquot of the dissolution liquid was mixed with 20 mL of the substrate-free KH perfusion medium and injected directly above the heart. In the global ischemia group, reperfusion was of the hearts was initiated ~10 s before injection of HP-[1,3-^{13}C]AcAc. ^{13}C NMR acquisition was initiated simultaneously with the injection of HP-AcAc. Serial FIDs were acquired using 20° pulses every 2 s. These data were processed using ACDLabs SpecManager (ACD/Labs, Canada). Peak areas were normalized to the total peak areas of all ^{13}C signals. Stacked hyperpolarized ^{13}C NMR spectra of the perfused hearts were generated using MATLAB (MATLAB R2017b; The MathWorks Inc.).

2.3 High-resolution NMR analyses of heart tissue extracts

The hearts were rapidly arrested and freeze-clamped after the ^{13}C NMR acquisition, approximately 3 min after the beginning of HP-AcAc injection. HR, CF, pO_2, and the developed pressure was measured before freeze-clamping the hearts. The frozen tissues were pulverized, extracted with perchloric acid (5%), neutralized, and reconstituted in D_2O containing 1 mM EDTA and 0.5 mM 2,2-dimethyl-2-silapentane-5-sulfonate (DSS, Chenomx Inc.) as in internal chemical shift standard. NMR data were acquired on a 14.1 T NMR spectrometer (Agilent). The concentration of β-hydroxybutyrate was calculated by fitting signal intensity of the methyl protons (C_4) using the Chenomx software with a pre-determined calibration curve.

2.4 Measurement of the NAD^+/NADH ratio in frozen tissue

In separate bench experiments where hearts were perfused under the same conditions, a 20 mg portion of left ventricle was excised from cold-arrested perfused hearts and washed three times with ice-cold PBS. The NAD^+/NADH ratios were determined using a commercially available kit (KA1657 Abnova, Taiwan) according to the manufacturer's protocol. Briefly, samples were homogenized with extraction buffer and centrifuged at 14,000 rpm for 5 min to remove cellular debris. Forty microliters of standard and sample solutions were analyzed in triplicate with a spectrophotometer at 565 nm. The NAD^+/NADH ratio was calculated as described by the manufacturer.

2.5 Transmission electron microscopy (TEM)

The morphology of the mitochondria was examined by TEM. After perfusion, a portion of left ventricle tissue was cut into 1 mm^3 pieces and fixed with 2.5% (v/v) glutaraldehyde in 0.1 M sodium cacodylate buffer. The tissue pieces were rinsed with the cacodylate buffer and post-fixed with 1% OsO_4 and 0.8% $K_3Fe(CN)_6$ in 0.1 M sodium cacodylate buffer for 1.5 h at room temperature. The fixed tissues were then rinsed with water and *en bloc*-stained with 4% uranyl acetate in 50% ethanol for two hours. The tissues were dehydrated by washing with increasing concentrations of ethanol and then infiltrated using Embed-812 resin mixed with propylene oxide and polymerized at 60°C overnight. Blocks were sectioned with a diamond knife (Diatome) on a Leica Ultracut 6 ultramicrotome (Leica

Microsystems) and collected onto copper TEM grids, post-stained with 2% aqueous uranyl acetate and lead citrate. Images were acquired on a Tecnai G2 Spirit transmission electron microscope (FEI) equipped with a LaB6 source using a voltage of 120 kV. Six random sections from each heart were examined for morphological analyses. A computerized point grid was digitally layered over the images. The mitochondrial cristae density and size were quantified as previously described [28]. All the analyses were performed in a blinded fashion.

2.6 Assessment of mitochondrial damage

Ultrastructural damage was evaluated with Flameng's scoring of the mitochondria.[29] For each study group, randomly selected 5 fields of view were analyzed per slice and each field included 20 mitochondria. The mitochondrial damage was categorized for each field using the following scoring system: Normal mitochondrial structure and intact granules, score 0; normal mitochondrial structure but absence of granules, score 1; swollen mitochondria with limpid matrix, score 2; ruptured cristae with limpid and concentrated matrix, score 3; and rupture cristae with incomplete inner and outer mitochondrial membranes, score 4. Mitochondrial scores from each of the 5 fields were calculated and represented as a mean ± standard deviation.

2.7 Statistical Analysis

Statistical analyses and plots were generated using GraphPad Prism v7 (GraphPad Software, San Diego, USA) and presented as mean ± SD. Statistical significance was tested using a two-tailed Student's *t*-test or analysis of variance (ANOVA) as appropriate. Statistical significance was denoted by $p < 0.05$ ($*p < 0.05$, $**p < 0.01$, $***p < 0.001$).

3. Results

3.1 Spin polarization levels and T_1 relaxation of HP [1,3-^{13}C]acetoacetate

A representative polarization buildup curve for [1,3-^{13}C]acetoacetate shown in Fig. 2b indicates that this molecule can be polarized quite quickly, with a comparable polarization buildup rate to that of sodium [1-^{13}C]pyruvate in a water/glycerol glassing matrix.[30] After dissolution, the measured ^{13}C signal enhancement of the carboxylate carbon was ~28,000-fold, corresponding to ~23% polarization (at 9.4 T). A comparison between hyperpolarized and thermally polarized ^{13}C NMR spectra of 2 mM [1,3-^{13}C]acetoacetate of the same sample are shown in Figure 2c. The T_1's of the carboxyl (C_1, 175.03 ppm) and ketone (C_3, 210.39 ppm) carbons measured in water at 9.4 T was 45 s and 37 s, respectively. It is important to point out that during the hydrolysis of ethyl [1,3-^{13}C]acetoacetate, a hydrolyzed product [1-^{13}C]acetate at 181.62 ppm and a decomposition product [2-^{13}C]acetone at 215.60 ppm were also produced in small amounts (Fig.S1). Three small peaks with resonance around 178–180 ppm reflect unknown impurities. The production of these byproducts was unavoidable using the prescribed hydrolysis conditions.

3.2 Physiology

Hearts in all experimental groups were perfused with a mixture of glucose, pyruvate, lactate, and long-chain fatty acids all at physiological concentrations for 20 min prior to an intervention. The experimental timeline is shown in Fig. 3a. During the first 20 min period,

oxygen consumption (MVO_2) and heart rates were found to be identical in all hearts (Fig. S2). After this initial perfusion period, each heart was subjected to one of two ischemic conditions or exposed to 20 μM rotenone prior to the HP experiment. After a 30 min intervention period, a single ^{31}P NMR spectrum was collected to measure levels of high-energy phosphates. Those spectra showed relatively constant ATP but variable P_i and PCr in each group (Fig. 3b). Given that the perfusate does not contain inorganic phosphate, the P_i signal, in this case, reflects only intracellular P_i so the chemical shift of this resonance could be used to measure intracellular pH.[31,32] The pH as measured by ^{31}P NMR was unchanged in the low-flow ischemia and rotenone-treated groups but was dramatically lower in global ischemic reperfusion hearts (Fig. 3c and Table 1). Heart rates, coronary flow, and MVO_2 were all lower at the end of the 30 min treatment period in the low-flow ischemia and rotenone-treated groups (Fig. 3c and Table 1). It was not possible to measure these same parameters in hearts after a 30 min period of global ischemia before reperfusion so measurements were taken after the hearts recovered.

3.3 Metabolism of hyperpolarized [1,3-^{13}C]acetoacetate

Hyperpolarized [1,3-^{13}C]AcAc was mixed with the perfusate containing multiple oxidizable substrates including long-chain fatty acids and injected to the perfused hearts via cannulated aorta. A degree of HP [1,3-^{13}C]AcAc oxidation is inevitable, but long-chain fatty acids are expected as the major acetyl-CoA source for cardiac energy metabolism under the current experimental conditions (Fig. S3) [33]. Regardless, the oxidation of HP [1,3-^{13}C]AcAc should not affect the metabolism of HP [1,3-^{13}C]AcAc by β-HBDH given the relatively high concentration of HP [1,3-^{13}C]AcAc available to the hearts during the ^{13}C NMR acquisition window. A few seconds after HP-[1,3-^{13}C]AcAc was introduced, the signals of [1-^{13}C]β-HB (180.62 ppm) and [3-^{13}C]β-HB (doublet, 67.25 and 65.80 ppm) began to appear reflecting the enzymatic conversion of acetoacetate to hydroxybutyrate (Fig. 4a). Representative summed ^{13}C NMR spectra acquired over 70 s from hearts in each group are shown in Figure 4b. From the summed spectra, more intense β-HB signals were apparent in hearts from the global ischemic reperfusion, low-flow ischemic, and rotenone-treated groups compared to controls. This observation is consistent with higher levels of mitochondrial NADH in the three ischemic groups compared to controls but certainly does not prove that total NADH levels were higher in those tissues. Given that [1-^{13}C]acetate is generated to a small extent during the preparation of [1,3-^{13}C]acetoacetate from ethyl [1,3-^{13}C]acetoacetate (see Materials and Methods), signals from HP-[1-^{13}C]acetate and HP-[1-^{13}C]acetylcarnitine, formed from HP-[1-^{13}C]acetate, were also detected. Oxidation of HP-AcAc to acetyl-CoA, albeit minimal, is also expected to contribute to the signal of HP-[1-^{13}C]acetylcarnitine. Although the intensity of [1-^{13}C]acetylcarnitine differed in each group, there was no correlation with degree of ischemia in the three models because the amount of [1-^{13}C]acetate produced during dissolution was variable and not easily controlled. The kinetic curves for the production of HP-[1-^{13}C]β-HB from HP-[1,3-^{13}C]AcAc over ~120 s are compared in Figure 4c. In normoxic control hearts, the hyperpolarized signal of [1-^{13}C]β-HB reached maximum intensity at ~25 s before decaying due to T_1 relaxation. The other three groups of hearts produced more HP-[1-^{13}C]β-HB but the general shape of those kinetic curves were similar. The areas under the curves (AUC) for all groups are compared in Figure 4d. The amount of HP-[1-^{13}C]β-HB detected in each group fell in the order, low-

flow ischemia (3.8-fold over controls) > rotenone-treated (1.8-fold) > global ischemia reperfusion (1.5-fold).

3.4 Myocardial β-hydroxybutyrate in freeze-clamped tissue

To examine whether the HP-[1-^{13}C]β-HB signal detected by ^{13}C NMR reflects only newly formed [1,3-^{13}C]β-HB formed or total tissue β-HB, high-resolution ^{1}H NMR spectra were collected on tissue extracts of hearts freeze-clamped immediately after the HP experiment. Figure 5a illustrates the NMR simulations for the interpretation of ^{1}H NMR β-HB resonances. The methyl resonance of β-HB consists of a doublet from 3-bond J_{HH} coupling for the non-^{13}C enriched fraction of β-HB and a doublet of doublets reflecting both 3-bond J_{HH} and 2-bond J_{CH} couplings for the [1,3-^{13}C]β-HB fraction (Fig. 5a). Representative ^{1}H NMR spectra of the methyl resonance of β-HB in tissue extracts are shown in Fig. 5b and the absolute amounts of ^{12}C versus ^{13}C β-HB measured against an internal standard of DSS are summarized in Table 2. In control hearts, both endogenous β-HB (0.064 ± 0.045 μmol/g dw) and [^{13}C]β-HB (0.036 ± 0.004 μmol/g dw) were relatively low compared to that measured in hearts from the other groups. Total β-HB in the ischemic groups was higher by factors of 4.8-fold over control in all three experimental groups but the distribution of ^{12}C-β-HB *versus* ^{13}C-β-HB varied considerably. For example, both the global ischemia reperfusion and low-flow ischemia groups had equivalent amounts of total β-HB (0.450 μmol/g dw), but the majority of β-HB was in the form of ^{12}C-β-HB (80%) in the global ischemic reperfusion hearts while the majority of β-HB was in the form of ^{13}C-β-HB in the low-flow ischemic hearts (91%). These percentages parallel the measured AUC values for production of HP-β-HB (Fig. 4d). This indicates that most of the β-HB in the tissue extract was derived from endogenous sources of acetoacetate during the 30 min period of global ischemia followed by reperfusion but much less was generated from exogenous HP-[1,3-^{13}C]AcAc after it was delivered. It is important to point out that reperfusion in globally ischemic hearts was initiated shortly before the delivery of HP-[1,3-^{13}C]AcAc and continued until the hearts were freeze-clamped. During this transition period, the ischemic and hypoxic heart tissue was again supplied with oxygen delivered in the oxygenated perfusion solution. As a result, the mitochondria began recovering from a highly reduced towards a normal state and the mitochondrial redox state likely favored the conversion of β-HB conversion to AcAc by β-HBDH (Fig. 1). Conversely, in the low-flow ischemic group, these hearts were less hypoxic during the 30 min treatment period so little ^{12}C-β-HB was produced from endogenous sources of acetoacetate. However, this hypoxic state was maintained during the delivery of HP-AcAc until the hearts were arrested. Hence, a substantial amount of HP-β-HB was produced after introduction of exogenous HP-[1,3-^{13}C]AcAc. The ^{13}C contributions to the total β-HB in the rotenone-treated (68%) fell between these two extremes.

3.5 Enzymatic determination of the NAD^+/NADH ratio

The ratio of NAD^+/NADH was evaluated using standard enzymatic methods to evaluate whether the amount of ^{13}C-β-HB produced and detected by ^{13}C NMR parallels the mitochondrial redox state. The NAD^+/NADH ratio in control, global ischemia reperfusion, low-flow ischemia, and rotenone-treated hearts was 3.90 ± 0.51, 1.15 ± 0.08, 0.75 ± 0.17, and 1.23 ± 0.20, respectively, consistent with higher tissue NADH in all three experimental groups compared to controls (Fig. 5d). From these ratios, one can conclude that

mitochondria in low-flow ischemic hearts were most highly reduced ($P < 0.05$) followed by mitochondria in global ischemic reperfusion and rotenone-treated hearts (not significantly different). One can assume that the mitochondria in globally ischemic hearts were much more highly reduced during the ischemic insult but quickly recovered when presented with oxygen and HP-AcAc. Caution needs to be exercised, however, in correlating the NAD^+/NADH ratio with the amount of β-HB produced because the estimated NAD^+/NADH ratios reported here reflect the total NAD^+ and NADH, both free and bound forms, in the cytosol plus mitochondria.

3.6 Morphology of mitochondria of perfused hearts by TEM

To determine whether increased production of β-HB in the ischemic and rotenone-treated hearts are reflected in a loss of mitochondrial integrity, samples of left ventricle tissue from each group were examined by TEM (Fig. 6a). As shown in the top image, control hearts displayed a well-defined mitochondrial membrane and densely packed cristae with longitudinal orientation while different degrees of mitochondrial deformation was observed in tissues from global ischemia reperfusion, low-flow ischemia, and rotenone-treated hearts. To place semi-quantitative values on these observations, the Flameng's scoring method was applied to quantify mitochondrial fragmentation and structural integrity. Flameng's scoring is a standard method for the assessment of mitochondrial injury and frequently reported for mitochondrial ultrastructural evaluation in cardiac function following ischemia.[29,34,35] The Flameng's scores for control, global ischemic reperfusion, low-flow ischemic, and rotenone-treated hearts were 0.16 ± 0.32, 2.35 ± 0.32, 2.9 ± 0.25, and 2.55 ± 0.36, respectively (Fig. 6b). The mitochondria in control hearts featured appropriately arranged myocardial fibers, mitochondria with intact cristae and intact outer membrane whereas mitochondria from ischemic and rotenone-treated hearts showed disordered myocardial fibers, different degrees of swelling, ruptured cristae with limpid and concentrated matrix and some mitochondria without complete membranes. The highest Flameng's score was found for mitochondria in the low-flow ischemic group. It is interesting to note that the group of hearts with the highest Flameng's score (most damage), lowest NAD^+/NADH ratio (presumably highest accumulation of NADH), also produced the largest amount of HP-β-HB as observed by ^{13}C NMR. This suggests that production of HP-β-HB from HP-AcAc may ultimately prove to be a good biomarker of mitochondrial dysfunction.

4. Discussion

Mitochondrial dysfunction is intricately linked to the development of heart failure [36,37] and has been associated with diabetes [2], cancer [4], neurodegenerative [3] and other diseases [38]. The mitochondrial redox state as reflected by NAD^+/NADH is thought to parallel the bioenergetic status of mitochondria [39] yet there is no reliable *in vivo* imaging method available to monitor mitochondrial redox. The steady-state tissue levels of AcAc and β-HB have long been thought to reflect the redox state of mitochondria since β-hydroxybutyrate dehydrogenase (β-HBDH) only exists on the inner surface of the inner mitochondrial membrane [40–42]. Thus, any disruption in the electron transport chain that results in the accumulation of excess NADH should stimulate the production of β-HB as long as AcAc is available for reduction. Classically, the mitochondrial NAD^+/NADH ratio is calculated by

using the known equilibrium constant of the reaction catalyzed by β-HBDH and measured tissue levels of AcAc and β-HB [43]. Such measurements assume conversion of AcAc to β-HB catalyzed by β-HBDH is rapid and is at equilibrium [44]. Nevertheless, conversion of AcAc to β-HB as detected over the short time-window allowed by these hyperpolarized species may not reflect a true mitochondrial equilibrium of AcAc, NADH, β-HB, and NAD^+ due to regional heterogeneity and insufficient kinetic equilibration, but instead likely reflects a shift in mitochondrial redox state i.e. increased vs decreased NADH availability.

HP ^{13}C-acetoacetate was first reported as an imaging probe by Jensen *et al* [45]. In that study, ethyl [1,3-^{13}C]acetoacetate was used as a marker for decreased esterase activity in liver tumors but HP-βHB was not detected. Recently, Miller *et al.* investigated the metabolism of HP-[1-^{13}C]AcAc and HP[1-^{13}C]β-HB in isolated perfused rat hearts as well as *in vivo* [46]. This study demonstrated that metabolism of HP ^{13}C-ketones can be detected in the heart and several downstream metabolites of the HP ^{13}C- agents were observed. We first reported with preliminary results that it is possible to correlate altered mitochondrial redox in perfused rat hearts with the production of HP-βHB from HP-AcAc [47]. Later, von Morze *et al.* reported the use of HP-^{13}C labeled AcAc to assess renal mitochondrial redox in rats [48]. In that report, mitochondrial redox in the kidney was assessed based solely on the appearance of HP-βHB and no other analytical measurements were reported. In this study, global ischemic reperfusion and rotenone-treated hearts were included as extreme models of mitochondrial dysfunction. An extended period of oxygen deprivation in the global ischemia reperfusion model is known to result in accumulation of excess mitochondrial NADH [49] while rotenone is known to impair the electron transport chain and reduce the mitochondrial NAD^+/NADH ratio in hearts [50]. The NMR results presented here showed increased production of ^{13}C-β-HB in all groups but hearts in the low-flow ischemia group produced the most ^{13}C-enriched β-HB. The experimental results showed that the NAD^+/NADH ratio as measured in tissue extracts was indeed low in low-flow ischemic hearts compared to controls, consistent with high mitochondrial NADH. This was also reflected by the highest Flameng's score in the low-flow ischemia group. The significant loss of mitochondrial structural integrity in low-flow ischemic hearts than in controls is in agreement with the conversion of HP-AcAc to HP-β-HB. These combined observations suggest that production of HP-β-HB from HP-AcAc does indeed reflect the mitochondrial redox in low-flow ischemic heart tissue.

The rotenone-treated hearts produced the next most ^{13}C-β-HB as measured by ^{1}H NMR spectroscopy (Fig. 5b) and the second highest amount of HP-β-HB detected over the 2 min time-period after addition of HP-AcAc (Fig. 4d). Total tissue β-HB and the NAD^+/NADH ratio were similar in rotenone-treated and global ischemic reperfusion hearts but only the NAD^+/NADH ratio was slightly higher in rotenone-treated hearts compared to low-flow ischemia hearts. This again suggests that production of HP-β-HB in rotenone-treated hearts largely reflects the accumulation of mitochondrial NADH. In comparison, metabolism is quite different in the global ischemia reperfusion heart model. After 30 min of zero-flow, ATP was depleted by ~80% and intracellular pH_{in} had decreased to ~6.3. However, total tissue β-HB was no higher than that seen in the low-flow ischemia and rotenone-treated groups. This finding plus a similar NAD^+/NADH ratio indicates that only certain levels of NADH can accumulate in the complete absence of oxygen and, consequently, the amount of β-HB that can be formed is also limited. Upon reperfusion and exposure to HP-AcAc, the

global ischemic reperfusion hearts made nearly the same amount of HP-β-HB over 2 min as that seen in rotenone-treated hearts but produced very little ^{13}C β-HB in comparison to the ^{12}C β-HB at steady state. This again is consistent with the prior observations that the HP-β-HB signal collected over 2 min does indeed reflect the amount of accumulated mitochondrial NADH in tissue even in extreme conditions when the electron transport chain is not fully intact.

Given that the mechanisms of β-HBDH and LDH are similar (both occur via an ordered Bi Bi mechanism), [51] it is of interest to know whether one can form HP-β-HB from HP-AcAc by a simple exchange mechanism without net conversion of NADH to NAD$^+$. It has been shown that conversion of exogenous HP-[1-^{13}C]pyruvate to HP-[1-^{13}C]lactate in cells over the time-scale of a typical HP experiment does not necessarily reflect stoichiometric conversion of pyruvate to lactate because exchange of label can occur rapidly in the active site of LDH without net conversion of pyruvate to lactate [24,26]. Timm *et al.* reported that a signal from HP-β-HB was detected in a suspension of EL4 muring lymphoma cells after injection of HP-AcAc but only with addition of unlabeled β-HB to increase the tissue concentration of this metabolite [52]. This suggests that HP-β-HB is produced from HP-AcAc at least in EL4 cells via an exchange mechanism very much like that shown earlier for P↔L exchange. It is important to stress that the appearance of HP-lactate and HP-β-HB should still reflect cytosolic and mitochondrial redox state regardless of whether the HP ^{13}C signals of these metabolites were a result of a true metabolic flux or an isotopic exchange. Large preexisting lactate and β-HB pools should reflect reduced cytosolic and mitochondrial redox. HP-lactate and HP-β-HB produced from HP-pyruvate and HP-AcAc exchanging into these pools should therefore report redox states of these two cellular compartments.

The experimental results presented here show that the NAD$^+$/NADH ratio was about 4-fold lower in tissues from three different ischemic models compared to control heart tissue. Although the ratio differences between the three ischemic models were small, the ratio in low-flow ischemic tissue was significantly lower than those measured in global ischemic reperfusion tissues and rotenone-treated tissues while the latter two groups did not differ. However, it is also known that the redox carriers NAD$^+$ and NADH are largely bound to enzymes in tissues so the local concentration of these carriers in proximity to any given enzyme is difficult to determine. Blinova, *et al.*, observed three distinct fluorescence lifetimes and emission wavelengths for NADH in isolated mitochondria with the “free” unbound NADH making up 63% of the total NADH and the remaining 37% (two or more components) with emission characteristics consistent with immobilized NADH [7]. This means that the NAD$^+$/NADH ratios reported may here largely reflect mitochondrial NAD$^+$/NADH but likely do not reflect the amount of each carrier available to membrane-bound β-HBDH. This suggests that the amount of HP-β-HB generated over the ~2 min period following exposure to HP-AcAc most likely reflects the local concentration of NADH available to the enzyme even in tissues containing highly damaged mitochondria. A significant increase in HP-β-HB production from HP-AcAc in ischemic and rotenone-treated hearts were verified with β-HB production in heart tissue extracts and NAD+/NADH redox state. These observations imply that enzymatic conversion of AcAc to β-HB monitored using HP ^{13}C-NMR can be used as a diagnostic tool for detecting mitochondrial dysfunction in the heart.

In summary, we demonstrate here the use of HP ^{13}C MRS to monitor ^{13}C-AcAc/^{13}C-β-HB metabolism as an indicator of mitochondrial redox state and mitochondrial dysfunction in perfused rat hearts. The redox-dependent conversion between this metabolic pair in mitochondria may lead to the development of an imaging tool for redox imaging of the heart by hyperpolarized ^{13}C MRI.

Supplementary Material

Refer to Web version on PubMed Central for supplementary material.

Acknowledgments

Nicholas Carpenter, Xiaodong Wen, and Thomas Hever are acknowledged for technical support in the perfusion experiments.

Funding information

National Institutes of Health (NIH) USA, Grant/Award Numbers: 5R37-HL034557 (ADS) and 2P41-EB015908 (CRM), Department of Defense Prostate Cancer Research Program USA, Grant/Award Number: W81XWH-12-1-0134 (CK) and American Heart Association USA, Grant/Award Number: 18POST34050049 (GS).

Abbreviations

β-HB	β-hydroxybutyrate
β-HBDH	β-hydroxybutyrate dehydrogenase
AcAc	acetoacetate
ANOVA	analysis of variance
ATP	adenosine triphosphate
AUC	area under curve
HP	hyperpolarized
^{13}C MRS	carbon-13 magnetic resonance spectroscopy
^{13}C MRI	carbon-13 magnetic resonance imaging
DNP	Dynamic nuclear polarization
DSS	2,2-dimethyl-2-silapentane-5-sulfonate
[Gd^{3+}]	Gadoteridol
KH	Krebs Henseleit
LF ischemia	Low-flow ischemia
MVO_2	Myocardial oxygen consumption
NAD^+	Nicotinamide adenine dinucleotide

NADH	Nicotinamide adenine dinucleotide
NMR	Nuclear Magnetic Resonance
PCr	Phosphocreatine
P_i	Inorganic phosphate
Rot	Rotenone
TEM	Transmission electron microscopy

References

1. Lesnefsky EJ, Chen Q, Tandler B, Hoppel CL. Mitochondrial Dysfunction and Myocardial Ischemia-Reperfusion: Implications for Novel Therapies. Annu Rev Pharmacol Toxicol 2017;57(1): 535–565. doi: 10.1146/annurev-pharmtox-010715-103335. [PubMed: 27860548]
2. Lowell BB, Shulman GI. Mitochondrial dysfunction and type 2 diabetes. Science 2005;307(5708): 384–387. doi: 10.1126/science.1104343. [PubMed: 15662004]
3. Lin MT, Beal MF. Mitochondrial dysfunction and oxidative stress in neurodegenerative diseases. Nature 2006;443(7113):787–795. doi: 10.1038/nature05292. [PubMed: 17051205]
4. Modica-Napolitano JS, Singh KK. Mitochondrial dysfunction in cancer. Mitochondrion 2004;4(5–6):755–762. doi: 10.1016/j.mito.2004.07.027. [PubMed: 16120430]
5. Lesnefsky EJ, Moghaddas S, Tandler B, Kerner J, Hoppel CL. Mitochondrial dysfunction in cardiac disease: ischemia--reperfusion, aging, and heart failure. J Mol Cell Cardiol 2001;33(6):1065–1089. doi: 10.1006/jmcc.2001.1378. [PubMed: 11444914]
6. Stein LR, Imai S. The dynamic regulation of NAD metabolism in mitochondria. Trends Endocrinol Metab 2012;23(9):420–428. doi: 10.1016/j.tem.2012.06.005. [PubMed: 22819213]
7. Blinova K, Carroll S, Bose S, et al. Distribution of mitochondrial NADH fluorescence lifetimes: steady-state kinetics of matrix NADH interactions. Biochemistry 2005;44(7):2585–2594. doi: 10.1021/bi0485124. [PubMed: 15709771]
8. Sato K, Kashiwaya Y, Keon CA, et al. Insulin, ketone bodies, and mitochondrial energy transduction. FASEB J 1995;9(8):651–658. [PubMed: 7768357]
9. Veech RL. The determination of the redox states and phosphorylation potential in living tissues and their relationship to metabolic control of disease phenotypes. Biochem Mol Biol Educ 2006;34(3): 168–179. doi: 10.1002/bmb.2006.49403403168. [PubMed: 21638666]
10. Veech RL, Eggleston LV, Krebs HA. The redox state of free nicotinamide–adenine dinucleotide phosphate in the cytoplasm of rat liver. Biochemical Journal 1969;115(4):609. [PubMed: 4391039]
11. Veech RL, Guynn R, Veloso D. The time-course of the effects of ethanol on the redox and phosphorylation states of rat liver. Biochem J 1972;127(2):387–397. [PubMed: 4342558]
12. Chance B, Legallais V, Schoener B. Metabolically linked changes in fluorescence emission spectra of cortex of rat brain, kidney and adrenal gland. Nature 1962;195:1073–1075. [PubMed: 13878020]
13. Chance B, Schoener B. Correlation of oxidation-reduction changes of intracellular reduced pyridine nucleotide and changes in electroencephalogram of the rat in anoxia. Nature 1962;195:956–958. [PubMed: 13878022]
14. Chance B, Cohen P, Jobsis F, Schoener B. Intracellular oxidation-reduction states in vivo. Science 1962;137(3529):499–508. [PubMed: 13878016]
15. Asfour H, Wengrowski AM, Jaimes R 3rd, Swift LM, Kay MW. NADH fluorescence imaging of isolated biventricular working rabbit hearts. J Vis Exp 2012(65):4115. doi: 10.3791/4115. [PubMed: 22872126]
16. Brazhe NA, Treiman M, Faricelli B, Vestergaard JH, Sosnovtseva O. In situ Raman study of redox state changes of mitochondrial cytochromes in a perfused rat heart. PLoS One 2013;8(8):e70488. doi: 10.1371/journal.pone.0070488. [PubMed: 24009655]

17. Schroeder MA, Cochlin LE, Heather LC, Clarke K, Radda GK, Tyler DJ. In vivo assessment of pyruvate dehydrogenase flux in the heart using hyperpolarized carbon-13 magnetic resonance. Proceedings of the National Academy of Sciences 2008;105:12051–12056.

18. Nelson SJ, Kurhanewicz J, Vigneron DB, et al. Metabolic Imaging of Patients with Prostate Cancer Using Hyperpolarized [1–13C]Pyruvate. Science Translational Medicine 2013;5:198ra108–198ra108.

19. Cunningham CH, Lau JY, Chen AP, et al. Hyperpolarized 13C Metabolic MRI of the Human Heart: Initial Experience. Circ Res 2016;119(11):1177–1182. doi: 10.1161/CIRCRESAHA.116.309769. [PubMed: 27635086]

20. Ardenkjaer-Larsen JH, Fridlund B, Gram A, et al. Increase in signal-to-noise ratio of > 10,000 times in liquid-state NMR. Proc Natl Acad Sci U S A 2003;100(18):10158–10163. doi: 10.1073/pnas.1733835100. [PubMed: 12930897]

21. Christensen CE, Karlsson M, Winther JR, Jensen PR, Lerche MH. Non-invasive In-cell Determination of Free Cytosolic [NAD(+)]/[NADH] Ratios Using Hyperpolarized Glucose Show Large Variations in Metabolic Phenotypes. Journal of Biological Chemistry 2014;289(4):2344–2352. doi: 10.1074/jbc.M113.498626. [PubMed: 24302737]

22. Spielman DM, Mayer D, Yen YF, Tropp J, Hurd RE, Pfefferbaum A. In vivo measurement of ethanol metabolism in the rat liver using magnetic resonance spectroscopy of hyperpolarized [1–13C]pyruvate. Magn Reson Med 2009;62(2):307–313. doi: 10.1002/mrm.21998. [PubMed: 19526498]

23. Park JM, Khemtong C, Liu SC, Hurd RE, Spielman DM. In vivo assessment of intracellular redox state in rat liver using hyperpolarized [1-(13) C]Alanine. Magn Reson Med 2017;77(5):1741–1748. doi: 10.1002/mrm.26662. [PubMed: 28261868]

24. Day SE, Kettunen MI, Gallagher FA, et al. Detecting tumor response to treatment using hyperpolarized 13C magnetic resonance imaging and spectroscopy. Nat Med 2007;13(11):1382–1387. doi: 10.1038/nm1650. [PubMed: 17965722]

25. Jiang W, Lumata L, Chen W, et al. Hyperpolarized 15N-pyridine derivatives as pH-sensitive MRI agents. Sci Rep 2015;5:9104. doi: 10.1038/srep09104. [PubMed: 25774436]

26. Khemtong C, Carpenter NR, Lumata LL, et al. Hyperpolarized 13C NMR detects rapid drug-induced changes in cardiac metabolism. Magn Reson Med 2015;74(2):312–319. doi: 10.1002/mrm.25419. [PubMed: 25168480]

27. Moon RB, Richards JH. Determination of intracellular pH by 31P magnetic resonance. J Biol Chem 1973;248(20):7276–7278. [PubMed: 4743524]

28. Santulli G, Pagano G, Sardu C, et al. Calcium release channel RyR2 regulates insulin release and glucose homeostasis. J Clin Invest 2015;125(5):1968–1978. doi: 10.1172/JCI79273. [PubMed: 25844899]

29. Flameng W, Borgers M, Daenen W, Stalpaert G. Ultrastructural and cytochemical correlates of myocardial protection by cardiac hypothermia in man. J Thorac Cardiovasc Surg 1980;79(3):413–424. [PubMed: 6243726]

30. Lumata L, Merritt ME, Malloy CR, Sherry AD, Kovacs Z. Impact of Gd3+ on DNP of [1–13C]pyruvate doped with trityl OX063, BDPA, or 4-oxo-TEMPO. J Phys Chem A 2012;116(21):5129–5138. doi: 10.1021/jp302399f. [PubMed: 22571288]

31. Hoult DI, Busby SJW, Gadian DG, Radda GK, Richards RE, Seeley PJ. Observation of tissue metabolites using 31P nuclear magnetic resonance. Nature 1974;252(5481):285–287. doi: 10.1038/252285a0. [PubMed: 4431445]

32. Schroeder MA, Swietach P, Atherton HJ, et al. Measuring intracellular pH in the heart using hyperpolarized carbon dioxide and bicarbonate: a 13C and 31P magnetic resonance spectroscopy study. Cardiovasc Res 2010;86(1):82–91. doi: 10.1093/cvr/cvp396. [PubMed: 20008827]

33. Jeffrey FM, Diczku V, Sherry AD, Malloy CR. Substrate selection in the isolated working rat heart: effects of reperfusion, afterload, and concentration. Basic Res Cardiol 1995;90(5):388–396. [PubMed: 8585860]

34. Han JS, Wang HS, Yan DM, et al. Myocardial ischaemic and diazoxide preconditioning both increase PGC-1alpha and reduce mitochondrial damage. Acta Cardiol 2010;65(6):639–644. doi: 10.2143/AC.65.6.2059860. [PubMed: 21302669]

35. Hou J, Wang H, Li X, Zhu Y. Remifentanil functions in the adaptive protection of cardiac function following ischemia. Exp Ther Med 2017;13(4):1514–1520. doi: 10.3892/etm.2017.4124. [PubMed: 28413502]
36. Burgoyne JR, Mongue-Din H, Eaton P, Shah AM. Redox signaling in cardiac physiology and pathology. Circ Res 2012;111(8):1091–1106. doi: 10.1161/CIRCRESAHA.111.255216. [PubMed: 23023511]
37. Mericskay M Nicotinamide adenine dinucleotide homeostasis and signalling in heart disease: Pathophysiological implications and therapeutic potential. Arch Cardiovasc Dis 2016;109(3):207–215. doi: 10.1016/j.acvd.2015.10.004. [PubMed: 26707577]
38. Pieczenik SR, Neustadt J. Mitochondrial dysfunction and molecular pathways of disease. Exp Mol Pathol 2007;83(1):84–92. doi: 10.1016/j.yexmp.2006.09.008. [PubMed: 17239370]
39. Canto C, Menzies KJ, Auwerx J. NAD(+) Metabolism and the Control of Energy Homeostasis: A Balancing Act between Mitochondria and the Nucleus. Cell Metab 2015;22(1):31–53. doi: 10.1016/j.cmet.2015.05.023. [PubMed: 26118927]
40. Churchill P, Mcintyre JO, Eibl H, Fleischer S. Activation of D-Beta-Hydroxybutyrate Apodehydrogenase Using Molecular-Species of Mixed Fatty Acyl Phospholipids. Journal of Biological Chemistry 1983;258(1):208–214. [PubMed: 6848496]
41. Churchill P, Mc Intyre JO, Vidal JC, Fleischer S. Basis for decreased d-β-hydroxybutyrate dehydrogenase activity in liver mitochondria from diabetic rats. Archives of Biochemistry and Biophysics 1983;224(2):659–670. doi: 10.1016/0003-9861(83)90253-9. [PubMed: 6347074]
42. McIntyre JO, Holladay LA, Smigel M, Puett D, Fleischer S. Hydrodynamic properties of D-β-hydroxybutyrate dehydrogenase, a lipid-requiring enzyme. Biochemistry 2002;17(20):4169–4177. doi: 10.1021/bi00613a010.
43. Williamson DH, Lund P, Krebs HA. The redox state of free nicotinamide-adenine dinucleotide in the cytoplasm and mitochondria of rat liver. Biochem J 1967;103(2):514–527. doi: 10.1042/bj1030514. [PubMed: 4291787]
44. Veech RL, Eggleston LV, Krebs HA. The redox state of free nicotinamide-adenine dinucleotide phosphate in the cytoplasm of rat liver. Biochem J 1969;115(4):609–619. [PubMed: 4391039]
45. Jensen PR, Serra SC, Miragoli L, et al. Hyperpolarized [1,3–13C2]ethyl acetoacetate is a novel diagnostic metabolic marker of liver cancer. Int J Cancer 2015;136(4):E117–126. doi: 10.1002/ijc.29162. [PubMed: 25156718]
46. Miller JJ, Ball DR, Lau AZ, Tyler DJ. Hyperpolarized ketone body metabolism in the rat heart. NMR Biomed 2018;31(6):e3912. doi: 10.1002/nbm.3912. [PubMed: 29637642]
47. Chen W, Khemtong C, Jiang W, Malloy CR, Sherry AD. Metabolism of hyperpolarized 13C-acetoacetate/β-hydroxybutyrate reveals mitochondrial redox state in perfused rat hearts. Proc Intl Soc Mag Reson Med 2016;24.
48. von Morze C, Ohliger MA, Marco-Rius I, et al. Direct assessment of renal mitochondrial redox state using hyperpolarized (13) C-acetoacetate. Magn Reson Med 2018;79(4):1862–1869. doi: 10.1002/mrm.27054. [PubMed: 29314217]
49. Varadarajan SG, An JZ, Novalija E, Smart SC, Stowe DF. Changes in [Na+](i), compartmental [Ca2+](,) and NADH with dysfunction after global ischemia in intact hearts. American Journal of Physiology-Heart and Circulatory Physiology 2001;280(1):H280–H293. [PubMed: 11123243]
50. Karamanlidis G, Lee CF, Garcia-Menendez L, et al. Mitochondrial complex I deficiency increases protein acetylation and accelerates heart failure. Cell Metab 2013;18(2):239–250. doi: 10.1016/j.cmet.2013.07.002. [PubMed: 23931755]
51. Tucker GA, Dawson AP. The kinetics of rat liver and heart mitochondrial beta-hydroxybutyrate dehydrogenase. Biochem J 1979;179(3):579–581. doi: 10.1042/bj1790579. [PubMed: 475768]
52. Timm KN, Kennedy BW, Brindle KM. Imaging Tumor Metabolism to Assess Disease Progression and Treatment Response. Clin Cancer Res 2016;22(21):5196–5203. doi: 10.1158/1078-0432.CCR-16-0159. [PubMed: 27609841]

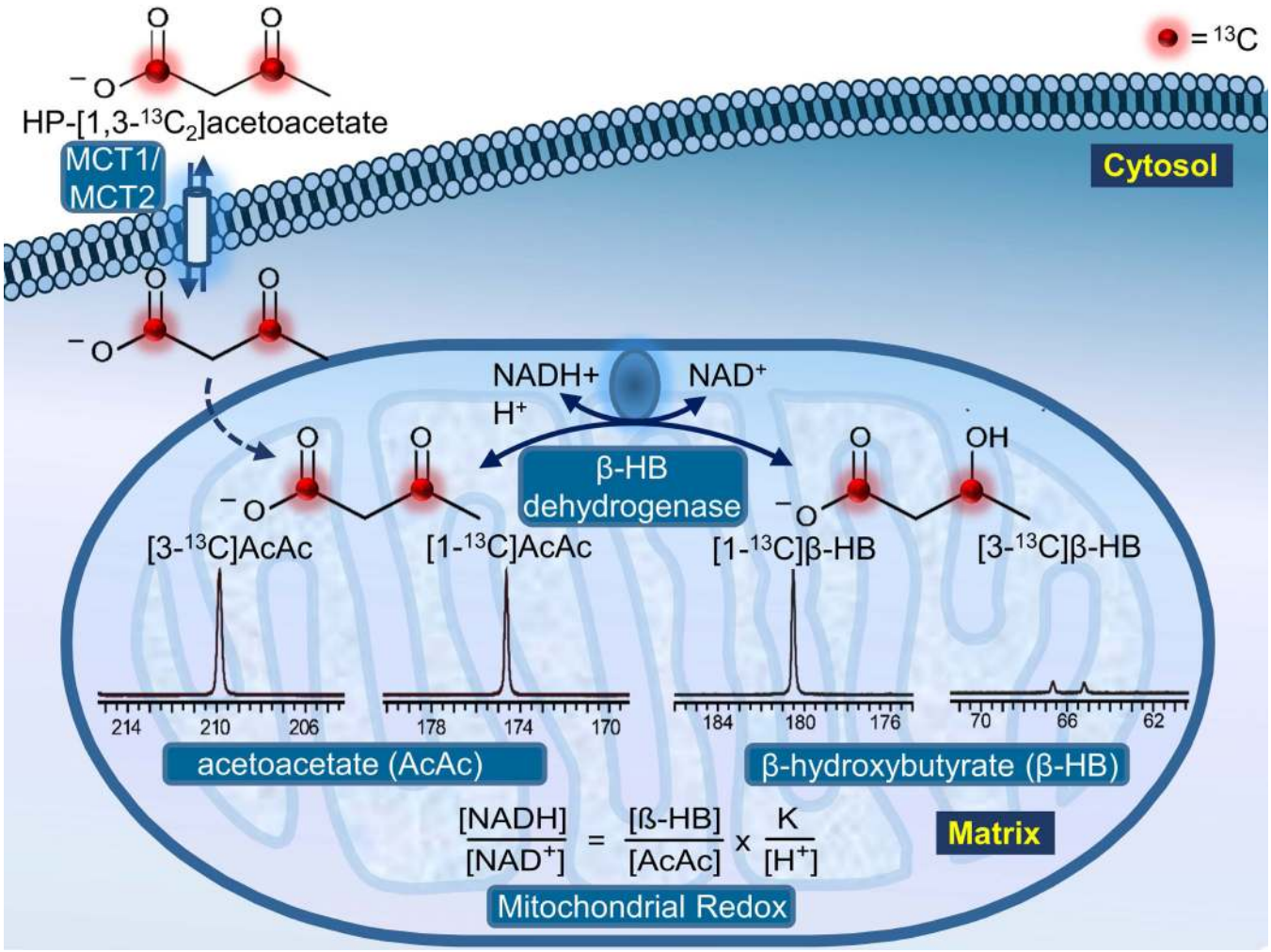

Figure 1.

An illustration showing the metabolism of acetoacetate to β-hydroxybutyrate by mitochondrial enzyme β-hydroxybutyrate dehydrogenase (β-HBDH). Chemical structures and ^{13}C-NMR resonances of HP [1,3-^{13}C]acetoacetate and [1,3-^{13}C]β-hydroxybutyrate are also shown.

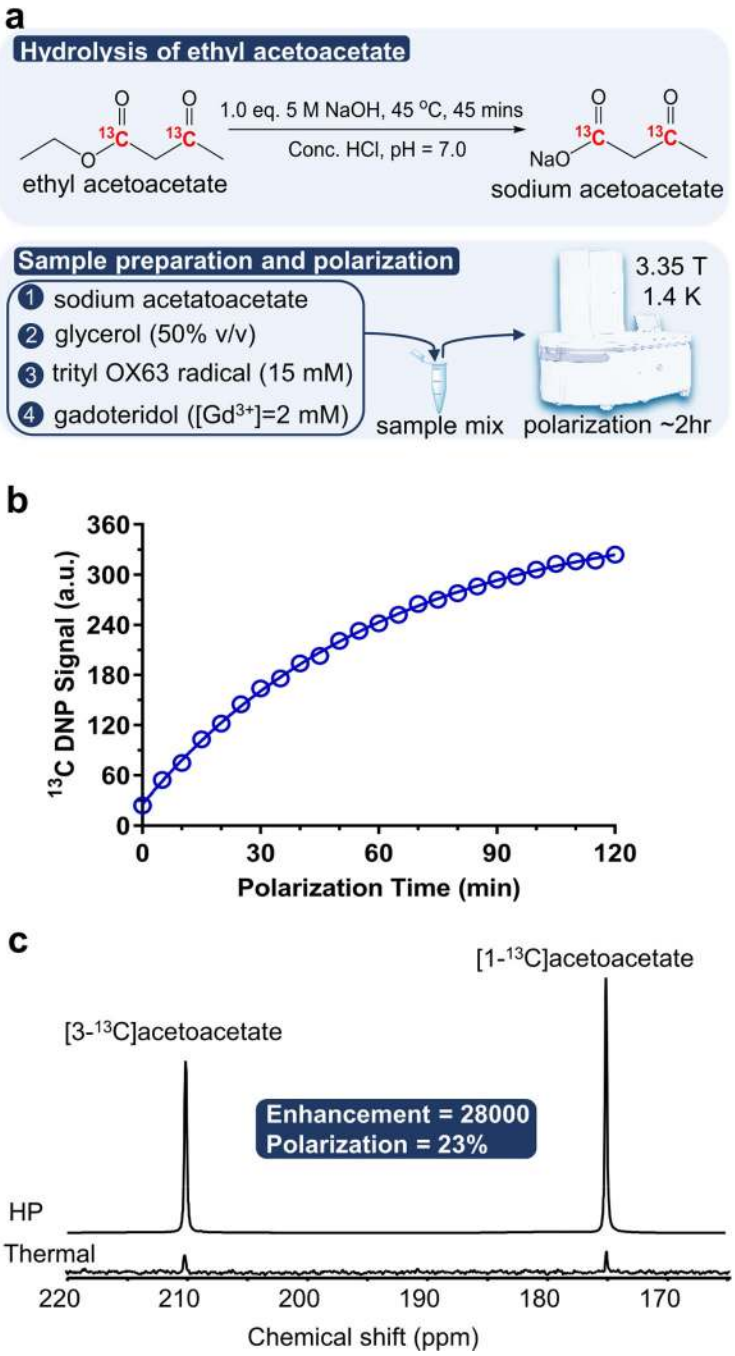

Figure 2.

(a) Reaction conditions for preparing [1,3-^{13}C]acetoacetate by hydrolysis of ethyl [1,3-^{13}C]acetoacetate and a scheme showing the hyperpolarization of [1,3-^{13}C]acetoacetate. *(b)* A representative buildup curve of [1,3-^{13}C]acetoacetate polarized in a HyperSense at 3.35 T and 1.4 K. *(c)* A single scan high-resolution ^{13}C NMR spectrum of [1,3-^{13}C]acetoacetate after ~ 2 h of hyperpolarization (*top*, flip angle = 10 deg). A single scan thermally polarized ^{13}C NMR spectrum (flip angle = 90 deg) of the same sample is

shown as the bottom spectrum, demonstrating the significantly improved sensitivity achieved by hyperpolarization.

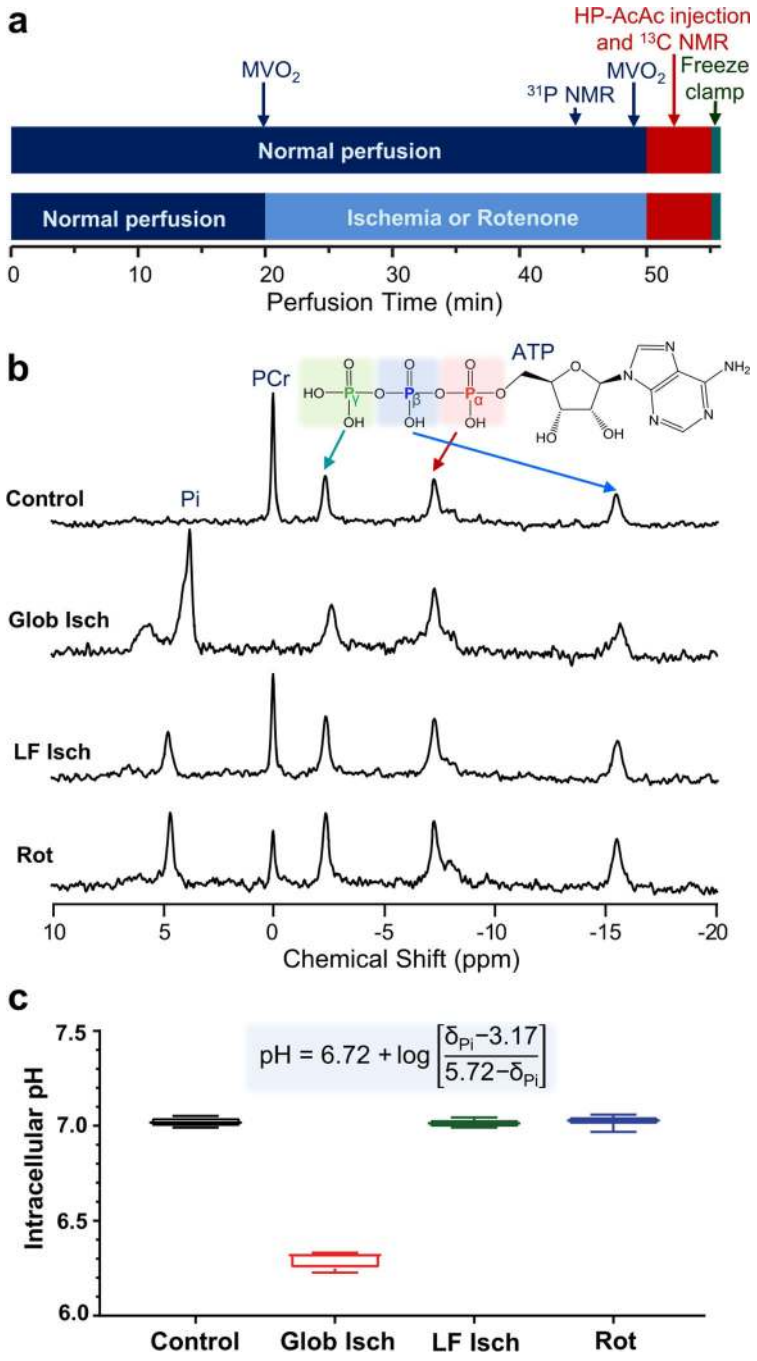

Figure 3.

(*a*) Perfusion diagrams for control hearts (top) and ischemic and rotenone-treated hearts (bottom) showing the perfusion timeline, HP-acetoacetate injection, and ^{13}C NMR acquisition; (*b*) representative ^{31}P NMR spectra of perfused hearts from different groups; (*c*) intracellular pH of the hearts during perfusion. pH was calculated from chemical shift of the inorganic phosphate (P_i) resonances using the displayed Henderson–Hasselbalch equation. Glob Isch = global ischemia reperfusion; LF Isch = Low-flow ischemia; Rot = Rotenone treatment.

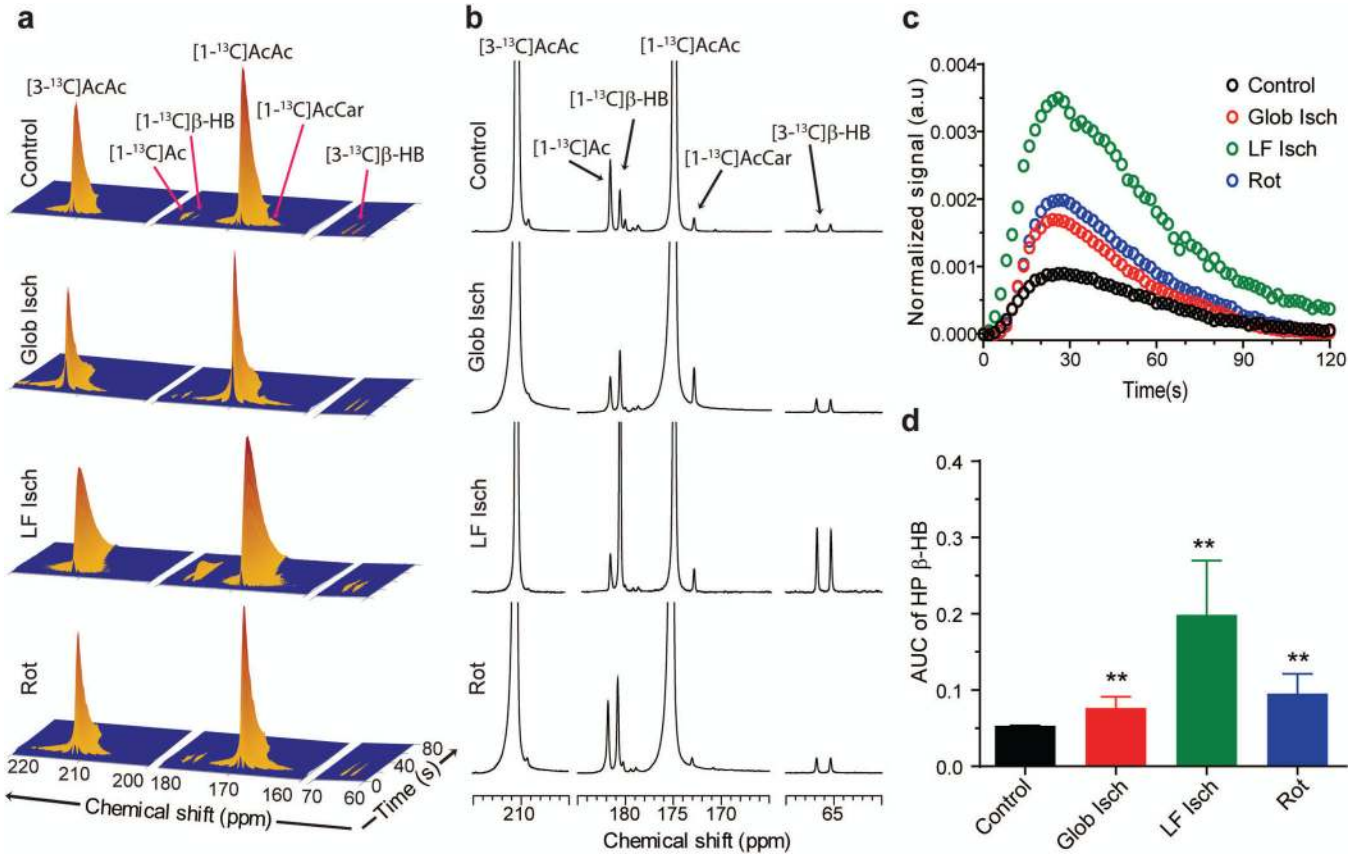

Figure 4.

(a) Representative real-time ^{13}C NMR signal evolution over time and *(b)* sum of thirty-five ^{13}C NMR spectra of perfused rat hearts after an injection of hyperpolarized [1,3-^{13}C]acetoacetate. (*c*) Average time-dependent signal intensities of HP [1-^{13}C]β-HB (n = 3) normalized over total HP ^{13}C signal. (*d*) Average area under the curve of the time-dependent HP [1-^{13}C]β-HB signal curves shown in *B*. A double asterisk (**) denotes statistical significance ($P < 0.005$) when compared with the control group. Glob Isch = global ischemia reperfusion; LF Isch = Low-flow ischemia; Rot = Rotenone treatment

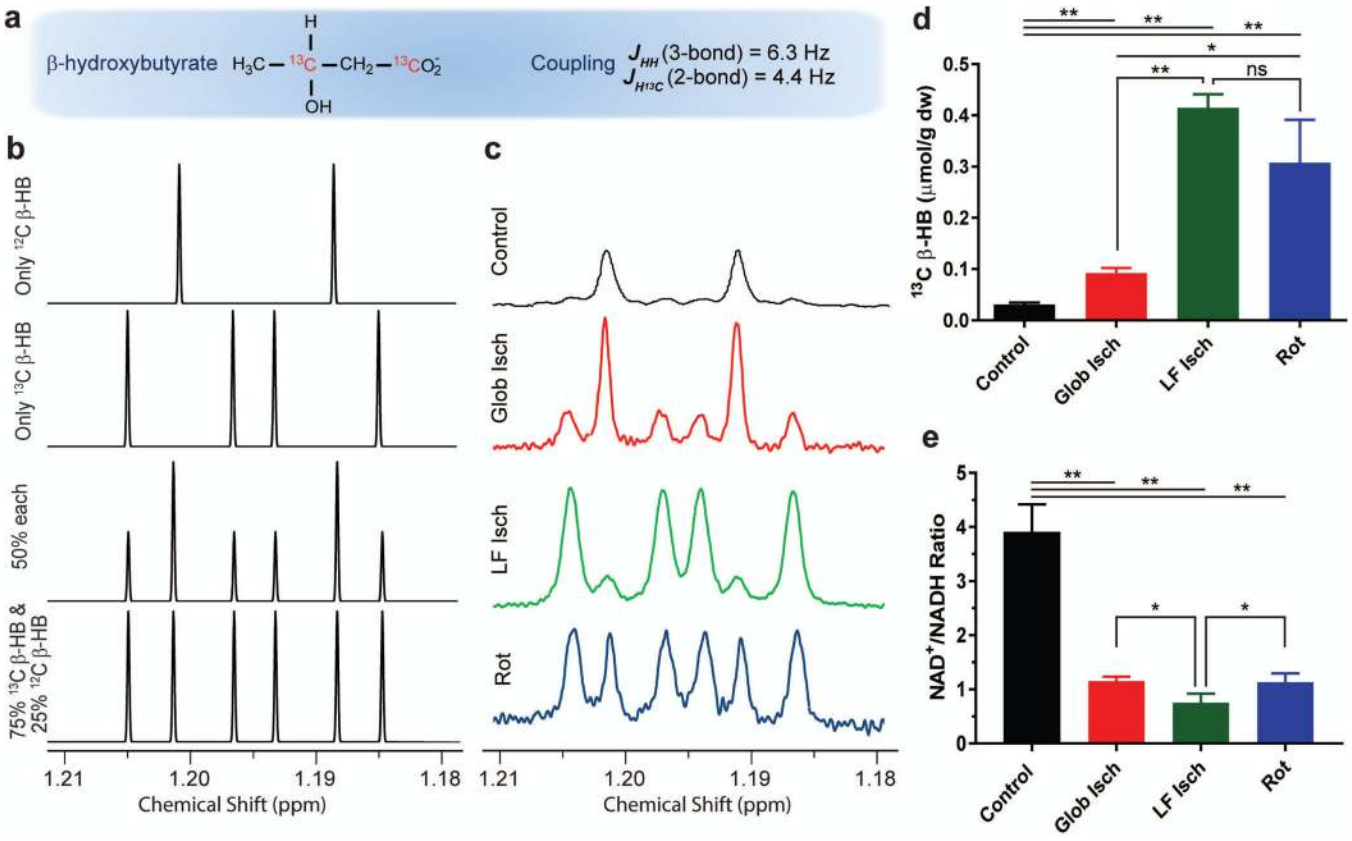

Figure 5.

(a–b) An illustration showing the interpretation of ^{1}H NMR spectral data from tissue extracts. The resonances are shown as doublet from 3-bond J_{HH} coupling for the non-^{13}C enriched fraction of β-HB and a doublet of doublets reflecting both 3-bond J_{HH} and 2-bond J_{CH} couplings for the [1,3-^{13}C]β-HB fraction. (*c*) Representative ^{1}H NMR spectra of tissue extract from hearts injected with hyperpolarized [1,3-^{13}C]acetoacetate, showing methyl protons of β-hydroxybutyrate. All spectra are presented under the same vertical scale using 0.5 mM DSS as a reference. Note that all hearts were freeze-clamped immediately after ^{13}C NMR. (*d*) Average tissue [1,3-^{13}C] β-hydroxybutyrate concentrations measured from ^{1}H NMR of heart tissue extracts. (*e*) NAD$^+$/NADH ratios measured from excised left ventricles of the hearts perfused under different conditions. A single and double asterisk denotes statistical significance with $P < 0.05$ and $P < 0.005$, respectively. ns denotes no significant difference.

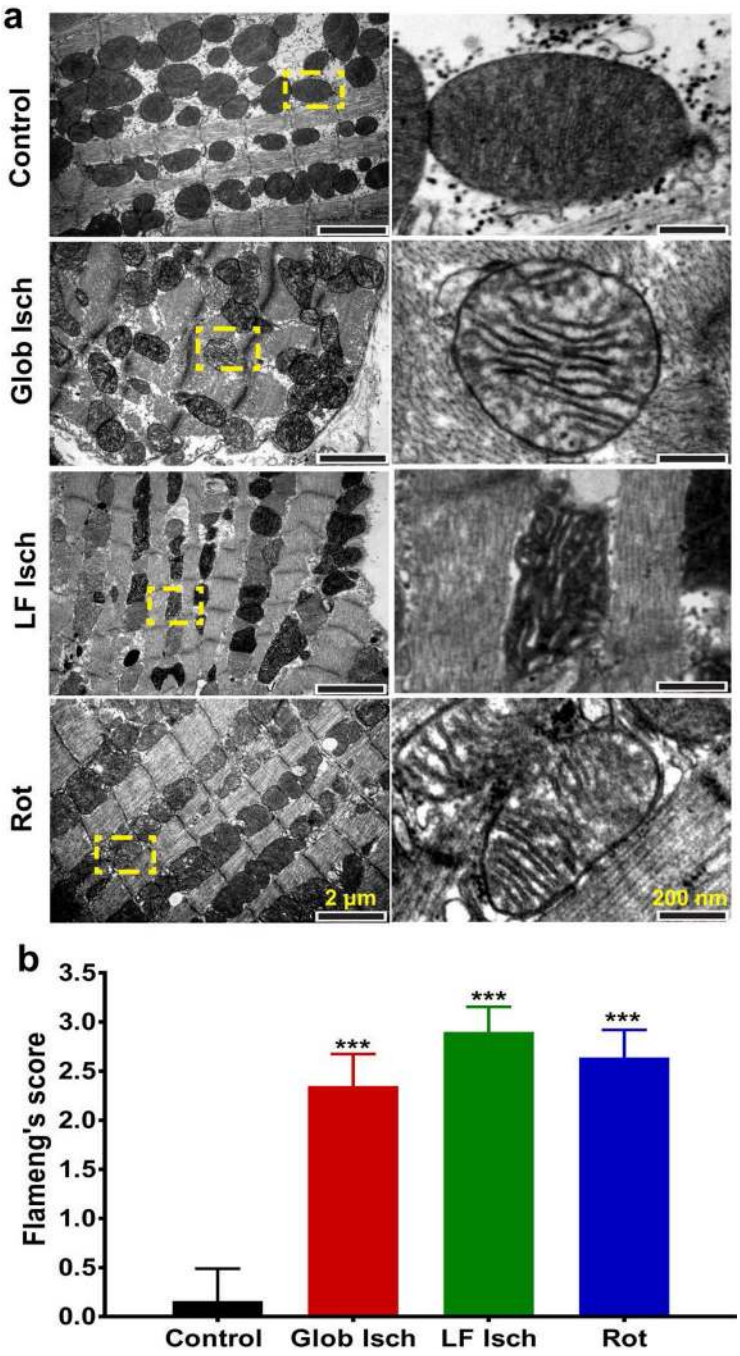

Figure 6.

(*a*) Transmission electron microscope (TEM) images of the left ventricle excised from isolated rat hearts from different perfusion conditions. Left panel images are low magnification micrographs. Images in the right panel are individual mitochondria showing various degrees of mitochondrial deformation in ischemic hearts. (*b*) The Flameng's mitochondrial scores obtained from morphological analyses of mitochondria.

Table 1.

Hemodynamic parameters of the hearts perfused under different conditions. Intracellular pH (pH_i) values were determined by ^{31}P NMR spectroscopy of the hearts from the resonance of inorganic phosphate (P_i) using phosphocreatine (PCr) as a reference. HR = heart rate; CF = coronary flow; MVO_2 = myocardial oxygen consumption

	Control	Global Ischemia[a]	Low-Flow Ischemia	Rotenone
Intracellular pH	7.02 ± 0.03	6.29 ± 0.05	7.02 ± 0.03	7.02 ± 0.05
HR, beats/min	268 ± 30	-	127 ± 49	128 ± 77
CF, mL/min	20.7 ± 5.4	-	5.5 ± 2.1	17.3 ± 5.5
MVO_2, μmol/min•g dw	19.94 ± 2.89	-	2.68 ± 2.14	2.08 ± 1.56

[a]HR, CF, and MVO_2 were not measured during global ischemia.

Table 2.

Average amounts of β-hydroxybutyrate (3 hearts per group) measured by ^{1}H NMR of heart tissue extracts. The values are presented in μmol per gram of dry tissue (μmol/g dw).

	Control	Global Ischemia	Low-Flow Ischemia	Rotenone
[βHB], μmol/ g dw				
^{13}C-βHB	0.031 ± 0.004	0.092 ± 0.010	0.415 ±0.0 26	0.308 ± 0.084
^{12}C-βHB	0.064 ± 0.045	0.363 ± 0.26	0.039 ± 0.016	0.141 ± 0.040
Total βHB	0.094 ± 0.041	0.455 ± 0.28	0.454 ± 0.039	0.449 ± 0.075